An Analytical Model of a New T-cored Coil Used for Eddy Current Nondestructive Evaluation

Siquan Zhang

Department of Electrical and Automation
Shanghai Maritime University, Shanghai, 201306, China
sqzhang@shmtu.edu.cn

Abstract ─ A model of an axisymmetric probe with a new T-core coil that can be used in eddy current testing is developed. The truncated region eigenfunction expansion (TREE) method is used to analyze the coil impedance problem of the T-core coil located above a multi-layer conductive material. First, the magnetic vector potential expressions of each region are formulated, then the coefficients of the magnetic vector potential are derived by using the boundary conditions, finally, the closed form expression of the coil impedance is obtained. The normalized impedance changes of the T-core coil caused by the presence or absence of the multi-layer conductor are calculated using Mathematica. The presented T-core coil is compared with I-core coil and air-core coil. The effects of the T-core parameter a_2, relative permeability μ_f and the thickness of the top section on the change in the coil impedance are discussed respectively. The analytical calculation results are compared with the results of finite element method, and the two agree very well, which verifies the correctness of the proposed T-core coil model.

Index Terms ─ Analytical model, coil impedance, eddy current testing, non-destructive evaluation, T-core coil, truncated region eigenfunction expansion.

I. INTRODUCTION

In eddy current testing (ECT), probes with ferrite cores of different shapes have been widely used to locate cracks, corrosion and other defects in multilayer conductive structures. Compared with the air-core coils, the ferrite-core coils have many advantages, such as concentrating magnetic flux, reducing magnetic flux loss and shielding external interference. Therefore, in eddy current detection, the ferrite-core coil probe can obtain a larger impedance change signal, so the defects in the conductor are easier to find and evaluate. I-core coils have already been investigated, and they can obtain better results than air-core coil in ECT [1-5]. Here we propose a new cored-coil as shown in Fig. 1, which is very similar to the I-core coil, here we call it T-core coil. The T-core coil can be obtained easily by adding a flat cylindrical core above the I-core, but the T-core has a better flux concentration effect than the I-core. On the other hand, if coils of the same size are used, the size of the T-core probe can be smaller than the C-core probe [6] and the E-core probe [7, 8]. No discussion related to T-core probes has been found in the literature, so it is necessary to investigate its application potential in ECT.

The problem of a T-core probe located above a layered half-space of conducting material is solved using the method of truncation region eigenfunction expansion (TREE) [9-11]. Azimuthal component of magnetic vector potential A_φ is expressed in the form of a series of orthogonal appropriate eigenfunctions involving discrete eigenvalues. Applying the Dirichlet boundary condition in the truncation surface is equivalent to a vanishing normal component of magnetic field. By truncating the solution domain, the solution can be expressed as a series form rather than as an integral. The most important advantage of the method is that by a careful selection of the discrete eigenvalues and the corresponding eigenfunctions, the field continuity can be satisfied at these different boundaries and interfaces simultaneously. And the numerical implementation is more efficient and the error control is easier. Firstly, a filamentary coil [12] was used in the analysis, then the expressions that describe the magnetic vector potentials of each region were derived. The closed form expression for the impedance of the T-core coil above the multi-layer conductor was obtained. The analytical calculation results obtained by the TREE method were compared with the finite element method (FEM) [13,14], which showed a very good agreement.

II. SOLUTION

The problem to be analyzed first is shown in Fig. 2. A filamentary coil excited by a harmonic current $Ie^{j\omega t}$ is wound around a T-core with relative magnetic permeability μ_f . The probe is located above a two-layer conducting half space with conductivity σ_6 and σ_7. The plane z = 0 coincides with the bottom of the core.

Submitted On: October 28, 2019
Accepted On: July 5, 2020

https://doi.org/10.47037/2020.ACES.J.350917

1054-4887 © ACES

According to the problem geometry, seven regions are formed. Using the Bessel functions J_n and Y_n, discrete eigenvalues were computed.

The eigenvalues q_i for regions 1, 5, 6, and 7 of Fig. 2 are the positive real roots of the equation:

$$J_1(q_i b) = 0\,, \tag{1}$$

where $J_1(x)$ is the Bessel function of the first kind. Because regions 2, 3, 4 comprise two sub-regions, the magnetic core and the air, so according to their radial dependences, the expressions of the magnetic vector potential for these two sub-regions can be analyzed as below.

For region 2:

$$A_{1core} = A_E J_1(m_i r), \quad 0 \le r \le a_2, \tag{2}$$

$$A_{1air} = A_E B_{1F} J_1(m_i r) + A_E C_{1F} Y_1(m_i r), \quad a_2 \le r \le b, \tag{3}$$

where m_i are the corresponding discrete eigenvalues.

Equations can be obtained from the continuity of B_r and H_z on the interface $r = a_2$, which yield the following expressions for B_{1F} and C_{1F}:

$$B_{1F} = \frac{\pi m_i a_2}{2}[J_1(m_i a_2)Y_0(m_i a_2) - \frac{J_0(m_i a_2)Y_1(m_i a_2)}{\mu_f}], \tag{4}$$

$$C_{1F} = \frac{\pi m_i a_2}{2} J_1(m_i a_2)J_0(m_i a_2)(\frac{1}{\mu_f} - 1)\,. \tag{5}$$

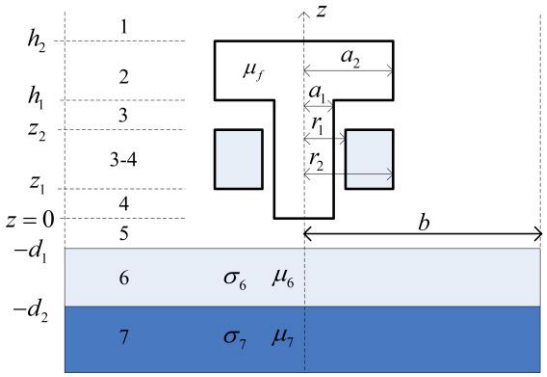

Fig. 1. Rectangular cross section T-core coil located above a layered conductive half-space.

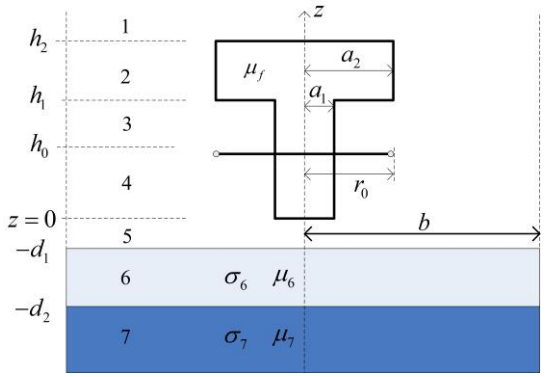

Fig. 2. Filamentary T-core coil located above a layered conductive half-space.

Since at the truncation boundary $r = b$, $A_\varphi(b, z) = 0$ must be satisfied, the following equation is obtained:

$$L_1(m_i b) = 0\,, \tag{6}$$

where

$$L_1(m_i r) = B_{1F} J_1(m_i r) + C_{1F} Y_1(m_i r)\,. \tag{7}$$

The eigenvalues m_i are the positive real roots of (6).

Using the same method to region 3 and 4 in Fig. 2, since the boundary condition must also be met, the following equation is formed:

$$R_1(p_i b) = 0\,, \tag{8}$$

where

$$R_1(p_i r) = B_{2F} J_1(p_i r) + C_{2F} Y_1(p_i r)\,, \tag{9}$$

$$B_{2F} = \frac{\pi p_i a_1}{2}[J_1(p_i a_1)Y_0(p_i a_1) - \frac{J_0(p_i a_1)Y_1(p_i a_1)}{\mu_f}], \tag{10}$$

$$C_{2F} = \frac{\pi p_i a_1}{2} J_1(p_i a_1)J_0(p_i a_1)(\frac{1}{\mu_f} - 1)\,. \tag{11}$$

The eigenvalues p_i are the real positive roots of (8).

The magnetic vector potential of each region was written as follows using matrix notation:

$$A_1(r, z) = J_1(\mathbf{q}^{\mathbf{T}} r)\mathbf{q}^{-1} e^{-\mathbf{q}z}\mathbf{C}_1, \tag{12}$$

$$A_2(r, z) = \begin{matrix} J_1(\mathbf{m}^{\mathbf{T}} r) \\ L_1(\mathbf{m}^{\mathbf{T}} r) \end{matrix} \mathbf{m}^{-1}(e^{-\mathbf{m}z}\mathbf{C}_2 - e^{\mathbf{m}z}\mathbf{B}_2) \quad \begin{matrix} 0 \le r \le a_2 \\ a_2 \le r \le b \end{matrix}, \tag{13}$$

$$A_3(r, z) = \begin{matrix} J_1(\mathbf{p}^{\mathbf{T}} r) \\ R_1(\mathbf{p}^{\mathbf{T}} r) \end{matrix} \mathbf{p}^{-1}(e^{-\mathbf{p}z}\mathbf{C}_3 - e^{\mathbf{p}z}\mathbf{B}_3) \quad \begin{matrix} 0 \le r \le a_1 \\ a_1 \le r \le b \end{matrix}, \tag{14}$$

$$A_4(r, z) = \begin{matrix} J_1(\mathbf{p}^{\mathbf{T}} r) \\ R_1(\mathbf{p}^{\mathbf{T}} r) \end{matrix} \mathbf{p}^{-1}(e^{-\mathbf{p}z}\mathbf{C}_4 - e^{\mathbf{p}z}\mathbf{B}_4) \quad \begin{matrix} 0 \le r \le a_1 \\ a_1 \le r \le b \end{matrix}, \tag{15}$$

$$A_5(r, z) = J_1(\mathbf{q}^{\mathbf{T}} r)\mathbf{q}^{-1}(e^{-\mathbf{q}z}\mathbf{C}_5 - e^{\mathbf{q}z}\mathbf{B}_5)\,, \tag{16}$$

$$A_6(r, z) = J_1(\mathbf{q}^{\mathbf{T}} r)\mathbf{u}^{-1}(e^{-\mathbf{u}z}\mathbf{C}_6 - e^{\mathbf{u}z}\mathbf{B}_6)\,, \tag{17}$$

$$A_7(r, z) = -J_1(\mathbf{q}^{\mathbf{T}} r)\mathbf{v}^{-1} e^{\mathbf{v}z}\mathbf{B}_7, \tag{18}$$

where

$$\mathbf{u} = \sqrt{\mathbf{q}^2 + j\omega\mu_6\mu_0\sigma_6}\,, \tag{19}$$

$$\mathbf{v} = \sqrt{\mathbf{q}^2 + j\omega\mu_7\mu_0\sigma_7}\,, \tag{20}$$

where J_i and Y_i are Bessel functions of i order. $J_1(\mathbf{q}^{\mathbf{T}} r)$, $J_1(\mathbf{m}^{\mathbf{T}} r)$, $L_1(\mathbf{m}^{\mathbf{T}} r)$, $R_1(\mathbf{p}^{\mathbf{T}} r)$ and $J_1(\mathbf{p}^{\mathbf{T}} r)$ are line vectors, $\mathbf{q}^{-1}, \mathbf{m}^{-1}, \mathbf{p}^{-1}, \mathbf{u}^{-1}, \mathbf{v}^{-1}$ and exponentials $e^{\pm\mathbf{q}z}$, $e^{\pm\mathbf{m}z}, e^{\pm\mathbf{p}z}, e^{\pm\mathbf{u}z}, e^{\mathbf{v}z}$ are diagonal matrices. $\mathbf{C}_i$ and $\mathbf{B}_i$ are column vectors of unknown coefficients.

Applying the interface conditions (continuity of B_z and H_r) between the seven regions of Fig. 2, the equations for calculation of the unknown vector coefficients can be obtained.

For the coil of rectangular cross-section shown in Fig. 1, the coil has width r_2-r_1, height z_2-z_1 and N wire turns, the magnetic vector potential A_φ in the various regions can be calculated using superposition in an integration form:

$$A(r,z)=\int_{r_1}^{r_2}\int_{z_1}^{z_2}A(r,z,r_0,z_0)dr_0dz_0\,. \tag{21}$$

Once the magnetic vector potentials of the regions 3, 4 and 3-4 in Fig. 2 are determined, the impedance of the coil in Fig. 1 can be calculated by integrating $rA_{3\text{-}4}$ over the cross section of the coil:

$$Z=\frac{j2\pi\omega i_0}{I^2}\int_{r_1}^{r_2}\int_{z_1}^{z_2}rA_{3-4}(r,z)drdz, \tag{22}$$

where

$$i_0=\frac{NI}{(r_2-r_1)(z_2-z_1)}. \tag{23}$$

The final expression of a T-core coil impedance can be obtained:

$$\begin{aligned}Z=&\frac{j\omega\mu\pi N^2}{(r_2-r_1)^2(z_2-z_1)^2}\chi(\mathbf{p}r_1,\mathbf{p}r_2)\mathbf{p}^{-4}\\&[2(z_2-z_1)\mathbf{p}+e^{\mathbf{p}(z_1-z_2)}-e^{\mathbf{p}(z_2-z_1)}\\&+\mathbf{W}_1\mathbf{W}_2^{-1}\mathbf{W}_3]\mathbf{p}^{-3}\mathbf{D}^{-1}\chi(\mathbf{p}r_1,\mathbf{p}r_2),\end{aligned} \tag{24}$$

where

$$\chi(x_1,x_2)=\int_{x_1}^{x_2}xR_1(x)dx\,, \tag{25}$$

$$\mathbf{W}_1=(e^{-\mathbf{p}z_1}-e^{-\mathbf{p}z_2})\mathbf{C}_{47}-(e^{\mathbf{p}z_2}-e^{\mathbf{p}z_1})\mathbf{B}_{47}\,, \tag{26}$$

$$\begin{aligned}\mathbf{W}_2=&(\lambda_1\mathbf{F}^{-1}\mathbf{G}+\lambda_2\mathbf{F}^{-1}\mathbf{G}^*)e^{-\mathbf{p}h_1}\mathbf{C}_{47}\\&-(\lambda_1\mathbf{F}^{-1}\mathbf{G}-\lambda_2\mathbf{F}^{-1}\mathbf{G}^*)e^{\mathbf{p}h_1}\mathbf{B}_{47},\end{aligned} \tag{27}$$

$$\begin{aligned}\mathbf{W}_3=&(\lambda_1\mathbf{F}^{-1}\mathbf{G}-\lambda_2\mathbf{F}^{-1}\mathbf{G}^*)(e^{\mathbf{p}(h_1-z_1)}-e^{\mathbf{p}(h_1-z_2)})\\&-(\lambda_1\mathbf{F}^{-1}\mathbf{G}+\lambda_2\mathbf{F}^{-1}\mathbf{G}^*)(e^{\mathbf{p}(z_2-h_1)}-e^{\mathbf{p}(z_1-h_1)}),\end{aligned} \tag{28}$$

$$\begin{matrix}\lambda_1\\ \lambda_2\end{matrix}=(\mathbf{T}-\mathbf{U})e^{\mathbf{m}(h_1-h_2)}\pm(\mathbf{T}+\mathbf{U})e^{\mathbf{m}(h_2-h_1)}\,, \tag{29}$$

$$\begin{matrix}\mathbf{B}_{47}\\ \mathbf{C}_{47}\end{matrix}=\frac{1}{2}(\mathbf{N}^{*-1}\mp\mathbf{H}^{-1})\mathbf{E}\mathbf{C}_{57}+\frac{1}{2}(\mathbf{N}^{*-1}\pm\mathbf{H}^{-1})\mathbf{E}\mathbf{B}_{57}\,, \tag{30}$$

$$\begin{aligned}\begin{matrix}\mathbf{B}_{57}\\ \mathbf{C}_{57}\end{matrix}=&\frac{1}{2}e^{\pm\mathbf{q}d_1}(\mu_6^{-1}\mp\mathbf{q}\mathbf{u}^{-1})e^{\mathbf{u}d_1}\mathbf{C}_{67}\\&+\frac{1}{2}e^{\pm\mathbf{q}d_1}(\mu_6^{-1}\pm\mathbf{q}\mathbf{u}^{-1})e^{-\mathbf{u}d_1}\mathbf{B}_{67},\end{aligned} \tag{31}$$

$$\begin{matrix}\mathbf{B}_{67}\\ \mathbf{C}_{67}\end{matrix}=\frac{1}{2}e^{\pm\mathbf{u}d_2}(\frac{\mu_6}{\mu_7}\pm\mathbf{u}\mathbf{v}^{-1})e^{-\mathbf{v}d_2}\,, \tag{32}$$

and

$$\mathbf{B}_{n7}=\frac{\mathbf{B}_n}{\mathbf{B}_7}\,, \tag{33}$$

$$\mathbf{C}_{n7}=\frac{\mathbf{C}_n}{\mathbf{B}_7}\,, \tag{34}$$

where **T**, **U**, **G**, **G***, **H** and **N*** are full matrices; **E**, **F**, and **D** are diagonal matrices, and they are defined as in [3], [4] and [6].

III. RESULTS AND DISCUSSIONS

The parameters in Table 1 were used in calculating the impedance of the T-core coil shown in Fig. 1. The proposed T-core coil is a new type of ECT probe, the parameters shown in Table 1 are set according to the parameters of the air-core coil and I-core coil in the references. The calculation was implemented in Mathematica using (24). In the calculations, the solution domain was truncated according to the parameter b = 60 mm, and the number of summation terms N_s = 60. The analytical calculation results were compared with the results of the finite element method. The Maxwell package was used, the meshes of triangles were 10866 and they can be refined using manual method.

In order to determine the discrete eigenvalues m_i and p_i, the FindRoot[] function was applied. The integral (25) was calculated using the expansion of the Struve and Bessel functions [2,10,15] by the aid of the BesselJ[], BesselY[] and StruveH[]. The matrices **D**, **F**, **H**, and **N*** were inverted using function Inverse[].

First, the impedances of the probes located above the layered conductor were calculated as $Z = R + jX$, then the conductor is removed ($\sigma_6 = \sigma_7 = 0$), the impedances of the probes were calculated as $Z_0 = R_0 + jX_0$. The changes in resistance and reactance were calculated as $\Delta R = R - R_0$ and $\Delta X = X - X_0$ respectively.

In order to verify the effectiveness of the proposed T-core coil in eddy current testing, the impedance changes of the I-core coil and the air-core coil were also calculated. In Fig. 1 and Fig. 2, when $a_2 = a_1$, the T-core becomes the I-core, so the I-core has the same inner core radius a_1, the same height h_2 and the same relative permeability μ_f = 500 with the T-core. If μ_f = 1, the ferrite-core coil becomes an air-core coil.

Table 1: Coil, core and conductor parameters used in calculation

Inner core radius	a_1	2 mm
Outer core radius	a_2	6 mm
Inner core height	h_1	6 mm
Outer core height	h_2	8 mm
Relative permeability	μ_f	500
Inner coil radius	r_1	2.2 mm
Outer coil radius	r_2	6 mm
Offset	z_1	0 mm
Parameter	z_2	5 mm
Number of turns	N	600
Liftoff	d_1	1 mm
Parameter	d_2	3 mm
Relative permeability	μ_6, μ_7	1
Conductivity	σ_6, σ_7	10 MS/m
Radius of the domain	b	60 mm

The calculations were performed for 31 different frequencies ranging from 100 Hz to 100 kHz. Figure 3 and Fig. 4 show the changes in resistance and reactance normalized in relation to reactance X_0 obtained from the analytical calculation and FEM for an air-core coil, an I-core coil and a T-core coil. As can be seen from the

figures, the calculated results of the TREE method agree with the FEM results very well. At the same excitation frequency, whether it is resistance or reactance, the impedance changes of the T-core coil are the largest among the three coils.

The inductances L_0 of the air-core coil, the I-core coil and the T-core coil are calculated as 1.769 mH, 4.219 mH, and 6.098 mH respectively. At the same excitation frequency, the T-core coil is more sensitive than the I-core coil and the air-core coil.

Figure 5 shows an impedance plane diagram for the frequency f varying from 100 Hz to 100 kHz. The calculation results of TREE method and FEM method can be matched accurately.

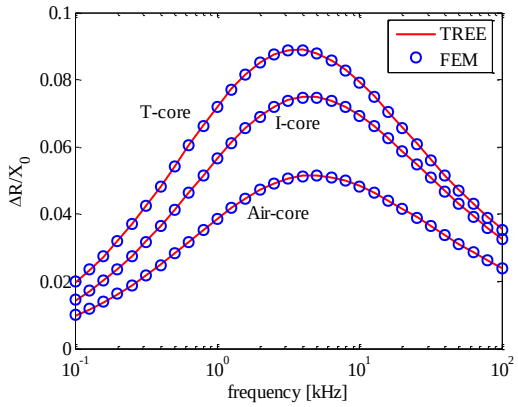

Fig. 3. Real part of the normalized impedance change as a function of frequency for an air-core coil (μ_f = 1), an I-core coil and a T-core coil (μ_f = 500).

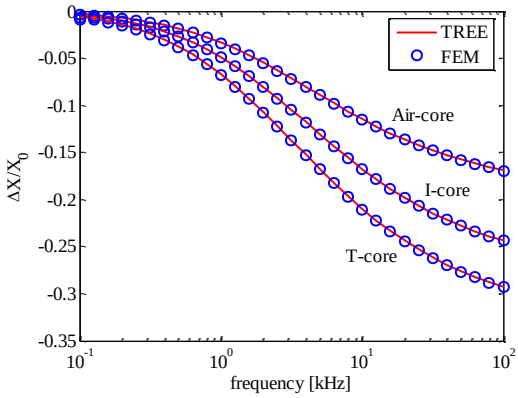

Fig. 4. Imaginary part of the normalized impedance change as a function of frequency for an air-core coil (μ_f = 1), an I-core coil and a T-core coil (μ_f = 500).

Table 2 shows the real parts of impedance change in a T-core coil obtained using FEM and TREE methods for several frequencies. The parameters used in the TREE method and the FEM method are the same as Table 1. In all cases, the relative errors between analytical results and FEM results are less than 0.5%, which shows they agree very well. If the truncated radius and the number of summation terms of the TREE method are increased, the accuracy of the calculation can also be improved. It took about 2 seconds to complete an impedance calculation using TREE method, which is less than the 4 seconds taken by the FEM on a computer with 3.70 GHz Pentium processor and 16 GB RAM. In the case of a large number of impedance calculations, the TREE method will show more advantage in computation speed than FEM.

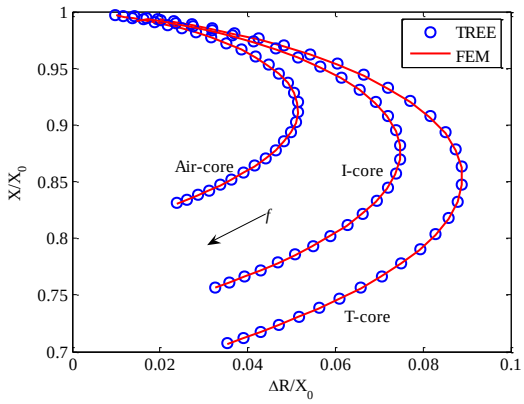

Fig. 5. Impedance plane diagram for an air-core coil (μ_f = 1), an I-core coil and a T-core coil (μ_f = 500) (frequency varying from 100 Hz to 100 kHz).

Table 2: Real part of impedance changes of a T-core coil obtained using FEM and TREE methods

***f* (kHz)**	**FEM (Ω)**	**TREE (Ω)**	**Error (%)**
0.5	1.04256	1.0378	-0.45
1	2.7598	2.7478	-0.43
5	16.8613	16.8048	-0.33
10	30.3275	30.2416	-0.28
100	135.5627	135.2262	-0.25

Figure 6 and Fig. 7 show the relationship between the impedance change in the T-core coil and the length of a_2. The change in the impedance of the T-core coil increases as the length of a_2 increases. When a_2 is approximately 4.4 mm, the T-core coil shows the maximum sensitivity, and then as a_2 increases, the sensitivity decreases gradually.

The influence of the relative permeability μ_f of the T-core on the change in coil resistance is shown in Fig. 8, where f = 4 kHz and a_2 = 6 mm. When the relative permeability μ_f of the T-core is less than 1000, the ΔR value increases significantly with the increase of μ_f, when the relative permeability μ_f of the T-core is greater than 1000, the ΔR value increases slowly with the increase of relative permeability.

The relationship between the thicknesses of the top

section of the T-core and the change in coil resistance is shown in Fig. 9, where $f = 4$ kHz, $a_2 = 6$ mm and $\mu_f = 500$. Although the ΔR will increase as the thickness of the top section of T-core increases, the size of the probe will increase accordingly. Therefore, a more appropriate choice is to make the thickness of the top section of the T-core consistent with the size of the other parts of the core.

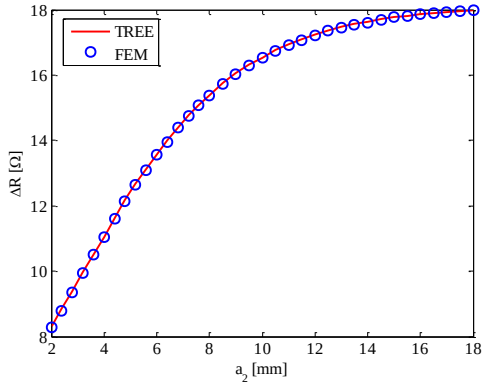

Fig. 6. Real part of the impedance change as a function of a_2 for a T-core coil ($\mu_f = 500$).

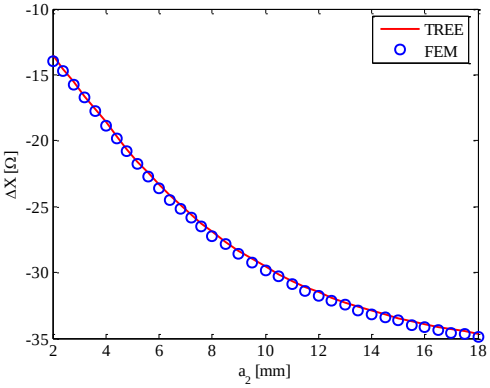

Fig. 7. Imaginary part of the impedance change as a function of a_2 for a T-core coil ($\mu_f = 500$).

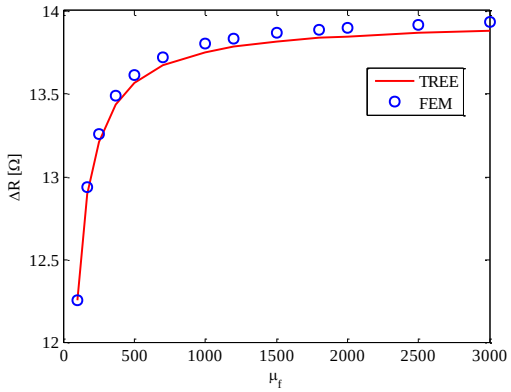

Fig. 8. Real part of the impedance change as a function of μ_f for a T-core coil.

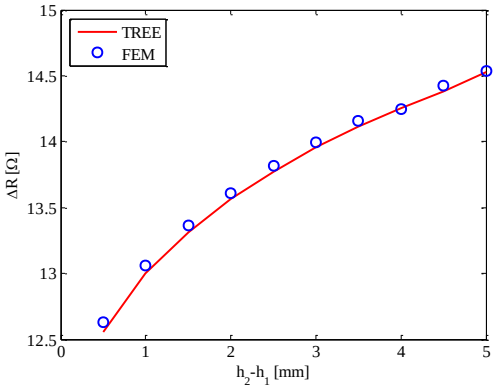

Fig. 9. Real part of the impedance change as a function of h_2-h_1 for a T-core coil.

IV. CONCLUSION

This paper presents an analytical model of a T-core coil placed over a multi-layer conductor. The final expression of the coil impedance obtained by the TREE method is in a closed form and can be fast implemented in softwares such as Mathematica or Matlab. The analytical model is verified by the finite element method. Compared with the I-core coil with the same inner core radius, the same height and the same relative permeability, the proposed T-core coil has higher magnetic flux concentration and shielding effect. The T-core can be used in the same probe together with the I-core to achieve better test results. The analytical T-core probe model can be used in computer simulation, or it can be directly applied in the detection of defects in multi-layer conductors. The solution also can be extended to more complex conductive structures with defects.

REFERENCES

[1] T. P. Theodoulidis, "Model of ferrite-cored probes for eddy current nondestructive evaluation," *J. Appl. Phys.*, vol. 93, no. 5, pp. 3071-3078, 2003.

[2] Y. Lu, J. R. Bowler, and T. P. Theodoulidis, "An analytical model of a ferrite-cored inductor used as an eddy current probe," *J. Appl. Phys.*, vol. 111, no. 10, pp. 103907-10, 2012.

[3] G. Tytko and L. Dziczkowski, "I-cored coil probe located above a conductive plate with a surface hole," *Measurement Science Review*, vol. 18, no. 1, pp. 7-12, 2018.

[4] G. Tytko and L. Dziczkowski, "An analytical model of an I-cored coil located above a conductive material with a hole," *The European Physical Journal Applied Physics.*, vol. 82, no. 21001, pp.1-7, 2018.

[5] Y. Li, Y. Wang, Z. Liu, I. M. Z. Abidin and Z. Chen, "Characteristics regarding lift-off intersection of pulse-modulation eddy current signals for evaluation of hidden thickness loss in cladded

conductors," *Sensors.*, vol. 19, no. 4102, pp. 1-14, 2019.

[6] H. Bayani, T. Theodoulidis, and I. Sasada, *Application of Eigenfunction Expansions to Eddy Current NDE: A Model of Cup-Cored Probes.* London, U.K.: IOP Press, pp. 57-64, 2007.

[7] F. Sakkaki and H. Bayani, "Solution to the problem of E-cored coil above a layered half-space using the method of truncated region eigenfunction expansion," *Journal of Applied Physics*, vol. 111, no. 7, pp. 2829-64, 2012.

[8] G. Tytko and L. Dziczkowski, "Calculation of the impedance of an E-cored coil placed above a conductive material with a surface hole," *Measurement Science Review*, vol. 19, no. 2, pp. 43-47, 2019.

[9] T. P. Theodoulidis and J. R. Bowler, "The truncated region eigenfunction expansion method for the solution of boundary value problems in eddy current non-destructive evaluation," *Rev. Progr. Quant. Non-Destruct. Eval.*, vol. 24A, pp. 403-408, 2004.

[10] T. P. Theodoulidis and E. E. Kriezis, *Eddy Current Canonical Problems (With Applications to Non-destructive Evaluation)*. Tech Sci. Press, Duluth, Georgia, pp. 106-121, 2006.

[11] F. Jiang and S. Liu, "Calculation and analysis of an analytical model for magnetic field monitoring based on TREE in eddy current testing," *Applied Computational Electromagnetics Society Journal*, vol. 33, no. 12, pp. 1489-1497, 2018.

[12] G. Tytko and L. Dziczkowski, "Fast calculation of the filamentary coil impedance using the truncated region eigenfunction expansion method," *Applied Computational Electromagnetics Society Journal*, vol. 33, no. 12, pp. 1461-1466, 2018.

[13] H. Zaidi, L. Santandrea, G. Krebs, Y. Le Bihan, and E. Demaldent, "FEM technique for modeling eddy-current testing of ferromagnetic media with small skin depth," *IEEE Trans. Magn.*, vol. 50, no. 2, pp. 129-132, 2014.

[14] B. Helifa, M. Féliachi, I. K. Lefkaier, B. Fouad, A. Zaoui, and N. Lagraa, "Characterization of surface cracks using eddy current NDT simulation by 3D-FEM and inversion by neural network," *Applied Computational Electromagnetics Society Journal*, vol. 31, no. 2, pp. 187-194, 2016.

[15] I. S. Gradshtein and I. M. Ryzhik, *Tables of Integrals, Series, and Products*. New York, Academic Press, 1980.

Siquan Zhang received the Ph.D. degree in Material Processing Engineering from the South China University of Technology, Guangzhou, China. His current research interests include eddy current testing, analytical model in non-destructive testing.